Antarctic density stratification and the strength of the circumpolar current during the Last Glacial Maximum

Jean Lynch-Stieglitz, Takamitsu Ito, Elisabeth Michel

AGU PUBLICATIONS

Paleoceanography

RESEARCH ARTICLE
10.1002/2015PA002915

Key Points:
- ACC transport co-varies with vertical and horizontal density stratification in models
- LGM data suggest modest increase in Southern Ocean density stratification and ACC transport

Supporting Information:
- Supporting Information S1

Correspondence to:
J. Lynch-Stieglitz,
jean@eas.gatech.edu

Citation:
Lynch-Stieglitz, J., T. Ito, and E. Michel (2016), Antarctic density stratification and the strength of the circumpolar current during the Last Glacial Maximum, *Paleoceanography*, *31*, 539–552, doi:10.1002/2015PA002915.

Received 11 DEC 2015
Accepted 19 APR 2016
Accepted article online 22 APR 2016
Published online 12 MAY 2016

Antarctic density stratification and the strength of the circumpolar current during the Last Glacial Maximum

Jean Lynch-Stieglitz[1], Takamitsu Ito[1], and Elisabeth Michel[2]

[1]School of Earth and Atmospheric Sciences, Georgia Institute of Technology, Atlanta, Georgia, USA, [2]Laboratoire des Sciences du Climat et de l'Environnement, CEA/CNRS-INSU/UVSQ, Gif-sur-Yvette Cedex, France

Abstract The interaction between ocean circulation and biological processes in the Southern Ocean is thought to be a major control on atmospheric carbon dioxide content over glacial cycles. A better understanding of stratification and circulation in the Southern Ocean during the Last Glacial Maximum (LGM) provides information that will help us to assess these scenarios. First, we evaluate the link between Southern Ocean stratification and circulation states in a suite of climate model simulations. While simulated Antarctic Circumpolar Current (ACC) transport varies widely (80–350 Sverdrup (Sv)), it co-varies with horizontal and vertical stratification and the formation of the southern deep water. We then test the LGM simulations against available data from paleoceanographic proxies, which can be used to assess the density stratification and ACC transport south of Australia. The paleoceanographic data suggest a moderate increase in the Southern Ocean stratification and the ACC strength during the LGM. Even with the relatively large uncertainty in the proxy-based estimates, extreme scenarios exhibited by some climate models with ACC transports of greater than 250 Sv and highly saline Antarctic Bottom Water are highly unlikely.

1. Introduction

The Antarctic Circumpolar Current (ACC) carries approximately 150 Sv (1 Sv = 10^6 m^3 s^{-1}) of water eastward around the Antarctic, vertically extending from the surface to the bottom of the Southern Ocean. The ACC is in thermal wind balance: the buoyancy force acting on the tilted density surfaces across the ACC (Figure 1) is balanced by the Coriolis force acting on the horizontal current. Today, this baroclinic transport (integrated thermal-wind transport referenced to zero bottom velocity) dominates the total ACC transport. The baroclinic portion of the ACC measured south of Australia is 147 ± 10 Sv [*Rintoul and Sokolov*, 2001], and the total transport estimated from inverse methods is 157 ± 10 Sv [*Ganachaud and Wunsch*, 2000].

1.1. Controls on ACC Transport

The ACC transport and the density stratification of the Southern Ocean are intimately linked to one another, but the thermal wind is merely a statement of balance and does not reveal the source of momentum or its response to different climate states. The overlying westerly winds impart zonal momentum into the ACC, which is balanced by the interfacial form stress and the topographic drag [e.g., *Allison et al*., 2010; *Johnson and Bryden*, 1989; *Masich et al*., 2015]. While it has long been thought that the ACC transport may scale with the wind stress, in recent years it has emerged that this picture is complicated by the importance of eddy activity in the Southern Ocean. Theoretical and modeling studies [*Hallberg and Gnanadesikan*, 2006; *Meredith and Hogg*, 2006; *Munday et al*., 2013] suggest that, in fact, the mean flow of the ACC (and thus its density stratification) is relatively insensitive to changes in wind strength over the Southern Ocean. In an idealized simulation with an eddy resolving model, *Munday et al*. [2013] show that when the strength of Southern Ocean westerly winds is varied between no winds at all and 5 times the modern value, only the variability of the ACC flow increases and the mean flow does not vary. Thus, the mean flow of the ACC is set not by the strength of the winds over the Southern Ocean, but rather by surface buoyancy fluxes and physical processes that control density stratification in this region [*Howard et al*., 2015; *Mazloff et al*., 2013; *Munday et al*., 2011].

1.2. ACC Transport During the LGM

Last Glacial Maximum (LGM) coupled ocean-atmosphere climate model simulations show a wide range in behaviors of the ACC transport, water mass distribution, and the overturning circulation. The simulated

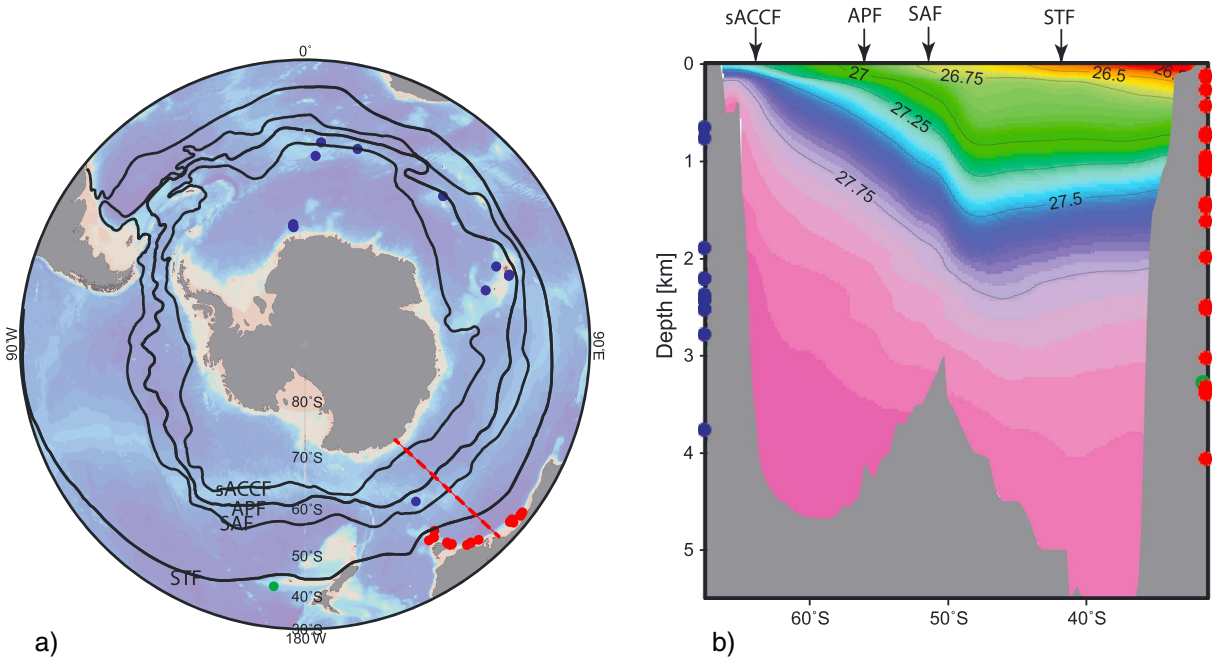

Figure 1. (a) Locations of data used in ACC density reconstruction (the red and blue dots are sediment core locations for the data shown in Figure 3, and the green dot is the location of the pore water measurements used to infer Lower Circumpolar Deep Water Density [*Adkins et al.*, 2002]. The solid black lines are the positions of the Antarctic Fronts [*Orsi et al.*, 1995]. (b) Present-day density structure south of Australia (σ_θ) [*Locarnini et al.*, 2013; *Zweng et al.*, 2013] with depth of sediment cores north (red) and south (blue) of the ACC marked; the dashed red line in Figure 1a shows the section shown in Figure 1b.

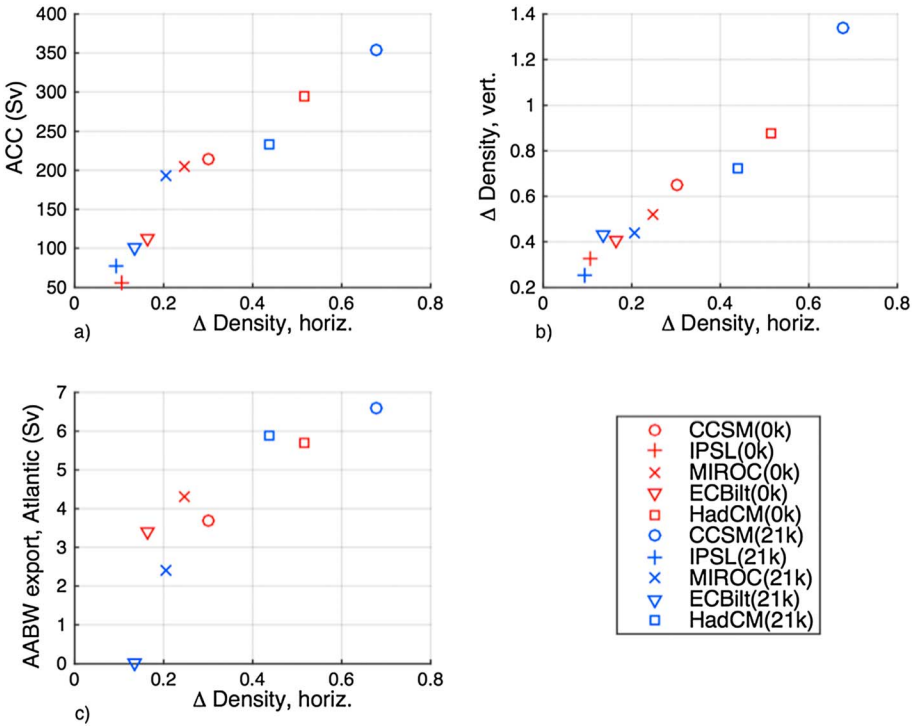

Figure 2. (a) Annual mean ACC transport (*y* axis, in Sv) is plotted against the (vertically and zonally averaged) meridional density difference (kg m^{-3}) between the two latitudes, north and south of the ACC at 40°S and 60°S for modern and LGM PMIP2 model simulations. (b) The vertical stratification (zonally averaged density difference between 0 and 3000 m at 40°S) is plotted against the meridional density difference (kg m^{-3}). (c) The volume flux of AABW into the abyssal Atlantic Ocean is plotted against the meridional density difference (kg m^{-3}). The value of AABW export is taken from Table 2 of *Weber et al.* [2007]. In all panels, the preindustrial condition is marked as (0 k) and the LGM (21 k).

LGM ACC transport among the Paleoclimate Model Intercomparison Project Phase 2 [*Braconnot et al*., 2007] (PMIP2) models shows a wide range from approximately 80 Sv to over 350 Sv, reflecting the equally wide range of density stratification (Figure 2). The coarse resolution of the ocean component of these models precludes the full, nonlinear representation of eddies, partly explaining the diverging climate sensitivities of the models.

McCave et al. [2014] used the grain size of the sortable silt fraction of the sediments from a series of sediment cores to infer bottom current speed across the ACC just downstream of the Drake Passage. While they found evidence for a decrease in bottom current in the southern portion of their transect, this is compensated by an increase in the northern portion, and they conclude that there was no net change in the strength of the ACC. However, recently published grain size measurements suggest a reductions in bottom speed at the northern edge of the Drake Passage and thus a slower ACC [*Lamy et al*., 2015]. In contrast, a study of the magnetic grain size in the Indian Ocean Sector suggests an increase in bottom speed for the Subantarctic ACC during the LGM [*Mazaud et al*., 2010].

The oxygen isotope ratio ($\delta^{18}O$) in tests of benthic foraminifera has been used as a proxy for seawater density in the upper ocean, as it reflects both temperature of calcification and the $\delta^{18}O$ of the seawater, in which the test calcified which in the upper ocean is well correlated with salinity [*Lynch-Stieglitz et al*., 1999]. In principle, we can estimate the density stratification across the LGM ACC, and thus, the LGM ACC transport, using oxygen isotope measurements in benthic foraminifera, provided that we are able to establish the relationship between foraminiferal $\delta^{18}O$ and density in this region. In this paper we will first explore the link between density stratification and circulation in the Southern Ocean using the climate model simulations. We will then use a compilation of paleoceanographic data, including foraminiferal $\delta^{18}O$ and reconstructions of seawater properties from pore waters, in order to estimate the Last Glacial Maximum density stratification and ACC transport in the Australian sector of the Southern Ocean. Finally, we will combine this new estimate with other data relevant to ACC strength and discuss the implications for LGM circulation and biogeochemistry.

2. Density and ACC Transport in PMIP Models

The output from preindustrial and Last Glacial Maximum (LGM) experiments for five climate models run under prescribed greenhouse gas concentrations and orbital parameters for the Paleoclimate Model Intercomparison Project 2 [*Braconnot et al*., 2007] (PMIP2) was analyzed. Paleoclimate model output for the preindustrial (0 k) and LGM (21 k) is obtained from the PMIP2 server at http://pmip2.lsce.ipsl.fr/. The climate models used here are Community Climate System Model version 3 [*Otto-Bliesner et al*., 2006], Institut Pierre Simon Laplace Climate Model version 4 [*Marti et al*., 2010], Model for Interdisciplinary Research on Climate version 3.2 [*Hasumi and Emori*, 2004], ECBilt/CLIO [*Goosse and Fichefet*, 1999; *Opsteegh et al*., 1998], and Hadley Centre Coupled Model version 3 [*Gordon et al*., 2000]. The eastward volume transport is first integrated vertically and then meridionally from Antarctica to the northern continental boundaries at three longitudes (Drake Passage, South Africa, and Australia). Taking a specific sector of the ACC transport does not change the overall picture, but we average the values from the three sectors with equal weights to derive broadly defined estimates of the ACC transport.

The models exhibit a wide range of behaviors, with modern day Antarctic Circumpolar Current (ACC) transport from approximately 50 to 300 Sv, with some of the models simulating stronger ACC during the LGM and some a weaker LGM ACC (Table S1 in the supporting information). To calculate the ACC transport, we first take the annual mean zonal velocity and integrate it vertically from bottom topography to the surface and then meridionally from the Antarctic to northern continental boundaries. We calculate the integrated volume transports at Drake Passage, South Africa, and Australia. The zonal transport south of Australia is approximately 20 Sv stronger than the Drake Passage/South Africa transport due to the additional mass flux to balance the Indonesian Throughflow. Among the PMIP2 models the density contrast across the ACC (40°S–60°S) is significantly correlated with the vertical density stratification in the north of the ACC (at 40°S, 0–3000 m) reflecting the geometrical link between vertical and horizontal stratification (Figures 2a and 2b).

2.1. Antarctic Bottom Water Formation, Atlantic Water Mass Structure, and ACC Transport

Reconstructions of stable carbon isotope and Cd/Ca in benthic foraminifera indicate the increased vertical extent of the Antarctic Bottom Water (AABW) and shoaling of the North Atlantic Deep Water (NADW) in

Table 1. ACC Transport South of Australia

Using Modern Oceanographic Data	
Full inverse methods [*Ganachaud and Wunsch*, 2000]	157 ± 10 Sv
Baroclinic transport referenced to bottom [*Rintoul and Sokolov*, 2001]	147 ± 10 Sv
Baroclinic transport refereced to 3 km using ocean margin data	130 Sv
Baroclinic transport referenced to 3 km, no Antarctic margin data	96 Sv
Using Core top foraminifera $\delta^{18}O$, same approximations as LGM study	
Baroclinic transport referenced to 3 km, no Antarctic margin data	98 Sv
Using LGM foraminifera $\delta^{18}O$ and pore water reconstructions	
Baroclinic transport referenced to 3 km, no Antarctic margin data	116 ± 52 Sv
Best estimate for LGM total transport	186 ± 83 Sv

the Atlantic Ocean during the LGM [*Curry and Oppo*, 2005; *Lynch-Stieglitz et al*., 2007; *Marchitto and Broecker*, 2006]. About half of the PMIP2 models have a shoaled boundary between the northern and southern deep-water circulation cells and the other half did not [*Weber et al*., 2007]. Some climate models that correctly reproduce the shoaling of the water mass boundary exhibit increased density contrast between northern- and southern-source deep waters [*Hesse et al*., 2011; *Otto-Bliesner et al*., 2006], where the higher density of the polar Southern Ocean increased the AABW formation, filling the greater fraction of the abyssal Atlantic basin. The extensive sea ice formation may have enhanced the extraction of buoyancy near the Antarctic coast, leading to the formation of saltier and denser AABW. In the analyzed models, the export rate of Antarctic Bottom Water (AABW) to the abyssal Atlantic Ocean is also significantly correlated to the density stratification [*Weber et al*., 2007] (Figure 2c). Those models that formed strongly saline AABW predicted intensified ACC transport with a strong density gradient across the ACC as explained by the thermal wind balance.

2.2. Using Models and Modern Data to Inform Strategy for Data-Based Reconstruction

Since, generally, it is only possible to estimate past density from proxy (sediment core and pore water) data for the LGM along the sea-floor, we first explore whether the changes in ACC transport in these model experiments can be adequately captured using ocean margin density information alone. Additionally, we limit the calculation of baroclinic transport to above 3.3 km, the depth at which there is no topographic barrier between the Antarctic and Australian continent, thus enabling a transport estimate from ocean margin data. The calculation is referenced to zero transport at this 3.3 km reference depth. Despite the wide range in predicted ACC transport, individual models show a transport that is largely baroclinic (Figure S1 in the supporting information). If we make a similar calculation using modern seawater properties along the Antarctic and Australian margin at 135°E [*Antonov et al*., 2010; *Locarnini et al*., 2010], we obtain a transport of 130 Sv, about 88% of the baroclinic transport referenced to the bottom using a full set of hydrographic data across the channel of 147 Sv [*Rintoul and Sokolov*, 2001] and 82% of the 157 Sv estimate of the total transport of the ACC [*Ganachaud and Wunsch*, 2000] (Table 1). Similarly, the models show baroclinic transport referenced to 3.3 km that is approximately 70% of the total transport and that changes in baroclinic transport scales with changes in the total transport.

Another limitation of the paleoclimate data is that there is little direct evidence with which to reconstruct the salinity and temperature (and thus density) along the Antarctic continental margin. However, given the demonstrated link between vertical stratification north of the ACC and horizontal stratification across the ACC (Figure 2), we explore the possibility of reconstructing changes in the ACC based only on density information north of the ACC. Today, the deep water along the Antarctic Margin has similar potential density as in the same water masses at greater depths to the north of the ACC (Figure 1). Since we have a pore water-based LGM density estimate for Lower Circumpolar Deep Water (LCDW) on the Chatham Rise in the South Pacific [*Adkins et al*., 2002], we recalculate the ACC transport using the modern water column data making the approximation that the waters along the Antarctic margin have the same properties as LCDW at the site of the pore water reconstructions. This results in a lower ACC transport than the calculation using the actual Antarctic margin density. There is a 26% reduction for the calculation using the World Ocean Atlas Climatology data on the Australian margin (Table 1) and an average 14% reduction for the data from the model simulations. However, with the exception of the models with very weak ACC, the transport changes in the models calculated from the Australian margin alone reflect the sense of the transport changes calculated with data from both margins (Figure S2).

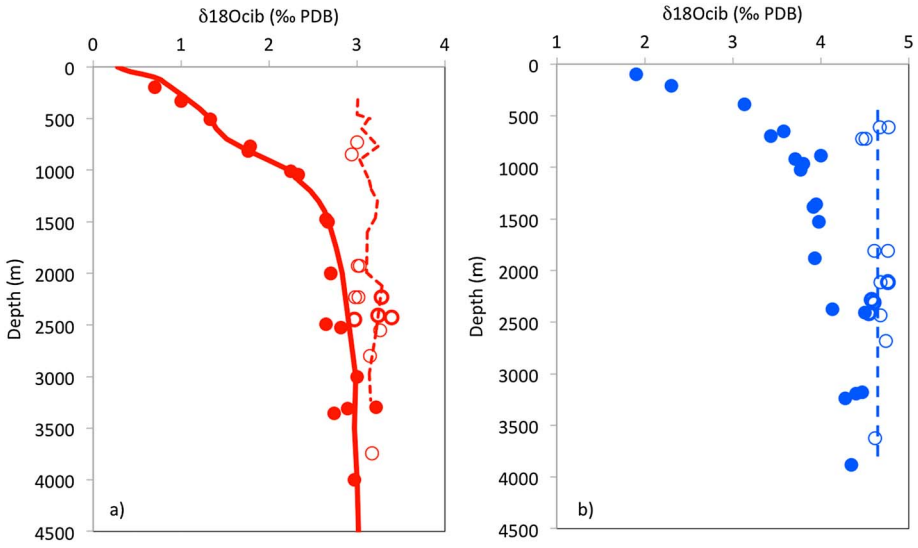

Figure 3. Oxygen isotope ratios in benthic foraminifera from both sides of the ACC from (a) core top and (b) Last Glacial Maximum sediments [*Duplessy et al.*, 2002; *Holbourn et al.*, 2002; *Lynch-Stieglitz and Fairbanks*, 1994; *Mackensen et al.*, 1989, 1993; *Mackensen*, 1994; *McCorkle et al.*, 1998; *Moy et al.*, 2006; *Ninnemann and Charles*, 2002; *Ott and Gersonde*, 1997a; 1997b; *Sikes et al.*, 2009]. The solid circles are data from north of the ACC (Australian margin) and are from *Cibicidoides* and *Planulina*. The heavy open circles are $\delta^{18}O$ data from south of the southern ACC Front. The lighter open circles are data from south of the Polar Front [*Orsi et al.*, 1995]. All water depths are shifted upwards by 120 m to account for lower sea level during the LGM. The red solid line is the predicted $\delta^{18}O$ value for foraminifera in the genera *Cibicidoides* and *Planulina* on the continental margin south of Australia based on the modern water column properties [*Locarnini et al.*, 2013; *Marchitto et al.*, 2014; *Ostlund et al.*, 1987; *Zweng et al.*, 2013]. The red dashed lines is the predicted $\delta^{18}O$ for foraminifera on the Antarctic margin south of Australia base on water column *T* and $\delta^{18}O$ [*Jacobs et al.*, 2005; *Schmidt et al.*, 1999]. The blue dashed line is the average value of the LGM foraminiferal $\delta^{18}O$ for the Antarctic sediment cores.

For our data-based LGM ACC transport reconstruction, we will use this approach. LCDW density will be inferred from the porewater-based temperature and salinity estimates at ODP Site 1123, and the density on the Australian Margin will be reconstructed using benthic oxygen isotope data and estimates of the *T*, *S*, and $\delta^{18}O$ of seawater along this margin.

3. Methods

We calculate the baroclinic transport of the ACC south of Australia above 3 km based on an estimate of the vertical density structure south of Australia and an assumed constant density along the Antarctic margin. Pore water-based temperature and salinity estimates of Lower Circumpolar Deep Water (ODP Site 1123) [*Adkins et al.*, 2002] are used to calculate density along the Antarctic margin. The vertical profile of seawater density south of Australia is calculating using temperature and salinity values estimated from $\delta^{18}O$ in glacial aged benthic foraminifera from a vertical transect of sediment cores from the southern margin of Australia (Figure 1). We establish the relationship between benthic foraminifera $\delta^{18}O$ and seawater temperature and salinity using paleoceanographic information from various sources and proxies. We also explore the sensitivity of this estimate to the assumed values by randomly sampling the various input parameters within the bounds of their probable values and recalculating the transport (Monte Carlo approach).

3.1. Oxygen Isotope Profiles From Benthic Foraminifera

We reconstruct vertical profiles of $\delta^{18}O$ from benthic foraminifera of the genera *Cibicidoides* and *Planulina* using recent and glacial aged sections of sediment cores from the continental margin south of Australia (Figure 3 and Table S2). All oxygen isotope data and age models for data from the Australian Margin have been previously published by a number of different groups [*Holbourn et al.*, 2002; *Lynch-Stieglitz and Fairbanks*, 1994; *McCorkle et al.*, 1998; *Moy et al.*, 2006; *Sikes et al.*, 2009]. Some of these studies included analyses on mixed species of *Cibicidoides* (which likely included some *wuellerstorfi*, which is sometimes assigned to the *Cibicidoides* genus), and some included *Planulina wuellerstorfi* alone as detailed in the original

references. Oxygen isotope ratios are reported as the *Cibicidoides* and *Planulina* values without additional species corrections. Data from older studies [*Lynch-Stieglitz and Fairbanks*, 1994; *McCorkle et al*., 1998] are corrected relative to the originally reported values to account for calibration issues in these laboratories that were discovered subsequent to publication [e.g., *Ostermann and Curry*, 2000], as well as differences in preparation procedures in some of the earlier studies ("roasting" samples prior to analysis, use of common acid bath preparation device). In both cases, the data are adjusted by an offset, bringing Holocene values from the study in line with expected values for these genera [*Marchitto et al*., 2014] and the data from the more recent publications. An offset of +0.32 is applied to data from *Lynch-Stieglitz and Fairbanks* [1994] and +0.30 to data from *McCorkle et al*. [1998]. The corrected values are in good agreement with newer data from the nearby Tasman Sea at similar water depths [*Ronge et al*., 2015]. We also re-analyzed samples from depths in the cores from the *Lynch-Stieglitz and Fairbanks* [1994] study, where sufficient *Cibicidoides* remained in our samples, and found a mean offset of 0.28 ± 0.04‰ (standard error, $n = 41$) relative to the earlier measurements at the same depths [*Lynch-Stieglitz*, 2015]. LGM water depth is corrected by subtracting 120 m to account for the global sea level drop.

We also compile the existing benthic oxygen isotope data from south of the ACC (Figure 3 and Table S3). We find only three cores in the literature with benthic oxygen isotope data from the Antarctic continental margin [*Mackensen et al*., 1989, 1993; *Mackensen*, 1994]. These data are from the species *Epistominella exigua*, and we apply a −0.42‰ correction before plotting to account for the offset in oxygen isotope ratios between this species and data from *Cibicidoides* and *Planulina* [*Labeyrie et al*., 1996]. We include two other cores from south of the southern ACC Front (sACCF), one from *Cibicidoides* and one from *E. exigua*, data corrected as above [*Ott and Gersonde*, 1997a, 1997b]. We also report some data from sediment cores, which are today near or south of the Antarctic Polar Front, but north of the southern boundary of the ACC (South ACC Front = sACCF) [*Orsi et al*., 1995]. These cores are today bathed by waters, which are not as dense as those on the continental margin as they are not fully south of the ACC, but if there were northward movement of the Antarctic frontal systems during glacial times may have been more fully south of the ACC. For one of these cores, the originally reported data [*Ninnemann and Charles*, 2002] have been corrected by +0.4 to account for interlaboratory calibration issues [*Hodell et al*., 2003]. The data from six additional cores from the Indian sector of the Southern Ocean were measured at the Laboratoire des Sciences du Climat et de l'Environnement (previously Centre des faibles Radioactivités) using methods described in the supporting information, and the down core data are reported in Table S4. Glacial-interglacial oxygen isotope differences from two of these cores have been published previously [*Duplessy et al*., 2002].

While we show the data from the Antarctic sediment cores in the figures, we do not use the oxygen isotope data from these Antarctic cores in our LGM ACC transport estimate. We cannot use these data to estimate the density on the Antarctic side of the ACC since we cannot constrain the relationship between the $\delta^{18}O$ of seawater and salinity during the LGM, which might have changed substantially due to changes in the cycling of freshwater via sea ice formation and melt.

3.2. Estimating LGM Seawater Density

Seawater density is a function of temperature, salinity, and pressure. While the effect of pressure is easily calculated from water depth, the lateral gradients in density that are needed to estimate the ACC flow depend on the temperature and salinity of seawater. Perhaps, the best estimates of past seawater temperature and salinity are based on the measurements of sediment pore fluid chlorinity and oxygen isotope ratios, which directly preserve information about the salinity and oxygen isotope ratios in seawater during glacial times. When combined with oxygen isotope measurements in benthic foraminifera, which reflect both the oxygen isotope ratio in seawater and the temperature of calcification, seawater temperature can be reconstructed as well [*Adkins et al*., 2002; *Schrag et al*., 2002]. However, these measurements are only available for a limited number of locations, primarily in deep waters.

Surface and thermocline temperature can be estimated from a number of different methods. Temperature estimates can be combined with the oxygen isotope ratio in foraminiferal calcite in order to reconstruct past seawater $\delta^{18}O$ ($\delta^{18}O_{sw}$). In the thermocline and upper ocean outside of polar areas, seawater $\delta^{18}O$ is related to salinity as changes in both quantities are driven by evaporation and precipitation [*Craig and Gordon*, 1965]. In the warm surface waters of the upper ocean, potential density and the $\delta^{18}O$ of foraminiferal calcite respond similarly to changes in temperature and freshwater forcing, and the $\delta^{18}O$ of calcite alone can be

used to estimate seawater density [*Lynch-Stieglitz et al*., 1999]. But in colder waters, it is critical to estimate temperature and salinity independently.

3.2.1. Density of Lower Circumpolar Deep Water

The density profile south of the ACC today is relatively uniform, and its vertical average likely reflects the most voluminous Lower Circumpolar Deep Water (LCDW), which spreads into the northern basins through the lower limb of the meridional overturning circulation (Figure 1). We make the approximation that LCDW temperature (*T*) and salinity (*S*) represent conditions along the Antarctic margin for our calculations of ACC transport (see section 2 above for a discussion of this approximation). We use pore fluid-based temperature and salinity reconstructions from Site 1123, which is located in South Pacific near New Zealand at 3290 m water depth [*Adkins et al*., 2002]. Recently published pore fluid measurements from a number of deep Pacific sites confirm that the salinity measured at Site 1123 (36.2‰) is representative of much of the deep Pacific between 3300 and 5800 m water depth [*Insua et al*., 2014]. Site 1123 is also relatively near the South Australian margin where we estimate the density profile north of the ACC.

3.2.2. Density Profile North of the ACC

The water column north of the ACC contains mode and intermediate waters in the upper ocean, as well as deep waters of various origins. The modern *T*-*S*-$\delta^{18}O_{sw}$ relationship shows that most of the column north of the ACC can be well approximated as a linear mixture of Subtropical Surface Water (STSW) and Antarctic Intermediate Water (AAIW) (0–1000 m water depth) or LCDW and AAIW (1000–3000 m water depth) (Figure S3). Our approach is to determine the *T*, *S*, and $\delta^{18}O_{sw}$ of each of these end-member water masses (LCDW, AAIW, and STSW) for the Holocene and the LGM. The predicted $\delta^{18}O$ for benthic foraminifera in the genera *Planulina* and *Cibicidoides* ($\delta^{18}O_{cib}$) is determined for each end-member using end-member $\delta^{18}O_{sw}$ and *T*. We then use the $\delta^{18}O_{cib}$ measurements from sediment cores taken from the continental margin south of Australia in order to establish the relative mixture of each end-member at each core site in the transect, and using the *T* and *S* of the end-members calculates density. It is assumed that the core of AAIW is located at 1000 m water depth during the LGM as it is today.

For the LCDW end-member we use the *T*, *S*, and $\delta^{18}O_{sw}$ estimates from Site 1123 [*Adkins et al*., 2002] as discussed above. Establishing the *T*, *S*, and $\delta^{18}O_{sw}$ of the AAIW and surface waters south of Australia is more complicated as no pore water measurements are available. We do have $\delta^{18}O_{cib}$ data at the water depth currently bathed by AAIW, and planktonic foraminiferal $\delta^{18}O$, which reflects conditions at the surface. The foraminiferal $\delta^{18}O$ is a function of temperature and the $\delta^{18}O_{sw}$ [*Marchitto et al*., 2014]:

$$\delta^{18}O_{cib} = \left(\delta^{18}O_{sw} - 0.27\right) + 3.58 - 0.245T + .0011T^2 \quad (1)$$

Given the $\delta^{18}O_{cib}$ and an independent estimate of temperature, we can then determine the $\delta^{18}O_{sw}$ of each end-member.

Elmore et al. [2015] present a 400 kyr low-resolution record of AAIW temperatures obtained from Mg/Ca measurements on the benthic foraminifera *Uvigerina perigrina*. For the LGM ($\delta^{18}O_{cib}$ = 3.8‰), they reconstruct AAIW temperatures of 2.1°C, about 3°C colder than modern temperatures at this core site. More generally, they find glacial values of about 2°C and interglacials values of up to 5°C at this site. We use a value of 2.1°C for the LGM temperature of AAIW off South Australia. The magnitude of the inferred temperature change is consistent with estimates of glacial-interglacial sea surface temperature change in the Subantarctic Zone, where AAIW is formed today. *Mashiotta et al*. [1999] estimate that the LGM temperature in the Subantarctic Pacific near where AAIW forms today was 2.5° cooler than present. Their estimate is based on the Mg/Ca of *Neogloboquadrina pachyderma* (left coiling), a cold-tolerant foraminifera that is likely to reflect the cold season conditions when AAIW forms. The LGM $\delta^{18}O$ of 3.8‰ for the *N. pachyderma* corresponds well to the AAIW $\delta^{18}O_{cib}$ value observed south of Australia reinforcing the idea that AAIW formed in this region during the LGM as it does today.

For the surface water end-member we refer to the compilation of *Bostock et al*. [2013], which expands on the MARGO database [*Waelbroeck et al*., 2009] in the region south of Australia. There are three sea surface temperature records from the Great Australia Bight north of 40°S with (one alkenone based and two based on foraminiferal assemblage data) [*Calvo et al*., 2007; *Passlow et al*., 1997], which show an average glacial temperature drop of 5°C. We therefore reduce the modern STSW end-member temperature by 5°C for our LGM analysis.

Today, the relationship between $\delta^{18}O_{sw}$ and salinity in surface and intermediate waters of the South Indian ocean is almost linear ($\delta^{18}O_{sw} = 0.607S–20.88$) (Figure S4). The linear relationship and slope are typical for surface waters in temperate regions of the world ocean [*Craig and Gordon*, 1965], as well as in the subsurface waters above the depth of AAIW in the tropical and temperate ocean, which gain their properties from the subduction of these temperate surface waters. If we assume that this linear relationship is a result of a mixture of salty subtropical gyre waters with a high-latitude freshwater end-member ($\delta^{18}O_{fw}$), a fresh end-member value of −20.9‰ is inferred:

$$\delta^{18}O_{sw} = \left(\delta^{18}O_{fw} + \left(\left(\delta^{18}O_{fw} - \delta^{18}O_{gyre}\right)/\left(S_{fw} - S_{gyre}\right)\right) * S \quad (2)$$

We will assume that the relationship between $\delta^{18}O_{sw}$ and salinity in the thermocline is controlled by similar processes during the LGM. If we combine equations (1) and (2) and assume that the freshwater end-member has a salinity of zero we obtain

$$S = \left(\delta^{18}O_{cib} + 0.27 - \left(3.58 - 0.245T + 0.0011T^2\right) - \delta^{18}O_{fw}\right)\left(-S_{gyre}\right)/\left(\delta^{18}O_{fw} - \delta^{18}O_{gyre}\right) \quad (3)$$

Given LGM $\delta^{18}O_{cib}$ and *T* for the end-member water masses, we can estimate salinity using equation (3) and independent estimates of $\delta^{18}O_{fw}$, $\delta^{18}O_{gyre}$, and S_{gyre}.

The $\delta^{18}O$ of the world ocean is estimated to have been higher by 1.0‰ [*Schrag et al*., 2002], and the salinity by 1.4 g/kg [*Insua et al*., 2014] during the LGM relative to the present. We thus increase the values of the subtropical gyre end-members (S_{gyre}, $\delta^{18}O_{gyre}$) by these amounts. Reconstructions of $\delta^{18}O_{sw}$ in the tropical Indian and Pacific oceans using Mg/Ca and oxygen isotope measurements on surface dwelling planktonic foraminifera [*Gibbons et al*., 2014] support the idea that subtropical surface water $\delta^{18}O$ changes were close to the whole ocean change of 1‰. There is no direct evidence (independent of $\delta^{18}O$) for changes in tropical salinity. However, we note that a pore water reconstruction from 1.4 km depth in the tropical Pacific shows a similar increase in salinity during the LGM as the deeper Pacific sites [*Adkins and Schrag*, 2003; *Insua et al*., 2014]. The fact that there is no discernable depth trend in reconstructed salinity from the LGM Pacific is consistent with the idea that intermediate water salinity changes were not drastically different from the global average.

Changes in the $\delta^{18}O$ of the freshwater end-member can be estimated from modeling studies, as supported by the changes in the $\delta^{18}O$ of precipitation archived in ice cores. In an atmospheric model which simulates the $\delta^{18}O$ of precipitation, *Risi et al*. [2010] show that the $\delta^{18}O$ of precipitation in the regions where the southern hemisphere thermocline is ventilated drops by 3–5‰ when this model is driven by LGM boundary conditions including sea surface temperatures from CLIMAP. This model result is supported by the ice core $\delta^{18}O$ record from Taylor Dome that shows a 3‰ decrease from the modern for the LGM [*Grootes et al*., 2001]. We therefore assume that the $\delta^{18}O$ of precipitation ($\delta^{18}O_{fw}$) was 4‰ lower than the modern value during the LGM (−24.9‰).

3.3. ACC Transport Estimate and Monte Carlo Error Estimate

Once we have established a best estimate vertical density profile south of Australia as described above, we combine it with our Antarctic margin density estimate from LCDW and calculate the baroclinic volume transport relative to a reference level of 3 km using today's average ACC latitude (56°S) for the Coriolis parameter. In order to make the best assessment of the reduction of ACC transport during the LGM relative to the modern, we compare it to a modern transport estimate using the same input parameters and methods as applied for the LGM (Table 1).

We assess the sensitivity of the ACC volume transport to the assumed and measured input parameters by estimating the uncertainty on each parameter (Table 2) and recalculating the transport by randomly resampling each input parameter within the assumed distributions. The latitude for the ACC transport is assigned a 1-sigma uncertainty of 2.5° to allow for the possibility of frontal movements of up to 5° latitude. It is expected that the ACC latitude was constrained by the bathymetry during the LGM as it is today. There is evidence for a northward position of the sea ice edge and temperature zonation [*Bostock et al*., 2013; *Gersonde et al*., 2005], but the data are not dense enough to detect the fronts (steep gradients) themselves. The uncertainties in the salinity and $\delta^{18}O_{sw}$ of LCDW at the Chatham Rise are taken from *Adkins et al*. [2002]. That study used the

Table 2. Parameter Values and Uncertainty Ranges Used in Transport Calculation

Parameter	Holocene	LGM	LGM 1-sigma Uncertainty
Endmember values:			
LCDW S	34.73 g/kg	36.19 g/kg	±.035 g/kg
LCDW $\delta^{18}O_{sw}$	0‰ SMOW	1‰ SMOW	±0.05‰
LCDW *T*	1.44°C	−1.1°C	function of errors in LCDW $\delta^{18}O_{sw}$ and $\delta^{18}O_{cib}$
STSW *T*	17.1°C	12.1°C	±1°C
AAIW *T*	4.59°C	2.1°C	±1°C
AAIW depth	1000 m	1000 m	±100 m
For 0–1000 m $\delta^{18}O_{sw}$ versus S relationship:			
$\delta^{18}O_{fw}$	−20.9‰ SMOW	−24.9‰ SMOW	±1‰
S_{gyre}	35.6 psu	37 psu	±0.14‰
$\delta^{18}O_{gyre}$	0.73‰ $\delta^{18}O_{sw} = 0.607S - 20.9$	1.73‰ SMOW $\delta^{18}O_{sw} = 0.72S - 24.9$	±0.1‰
For S. Australia profile:			
$\delta^{18}O_{cib}$	Table S2	Table S2	±0.07‰
For transport calculation:			
Latitude of ACC	56°S	56°S	±2.5°
ACC transport	98 Sv	116 Sv	±52 Sv

glacial-interglacial difference in $\delta^{18}O_{sw}$, in addition to the glacial-interglacial difference in $\delta^{18}O_{cib}$, to determine the LGM temperature. So we account for the fact that the error in temperature is not completely independent, but will be driven both by the error in $\delta^{18}O_{sw}$ and an additional error on the $\delta^{18}O_{cib}$ that they used in their calculation.

For the temperature of subtropical surface water at the Australian Margin, we assign a 1-sigma uncertainty of ±1°C based on the range of about 4°C in sea surface temperature estimates using different proxies in this region [*Bostock et al*., 2013]. For the temperature of AAIW at the Australian Margin we use a 1-sigma error of ±1°C, the calibration error on the temperature estimate using Mg/Ca in *Uvigerina* [*Elderfield et al*., 2012]. Another study using Mg/Ca in *Uvigerina* finds a larger LGM temperature change (−5°C) at 600 m water depth in the Drake Passage than is found at the Australian Margin. While this could be due to true oceanographic differences between these locations, it would support the use of this relatively large error estimate [*Roberts et al*., 2016]. We estimate an error of ±2‰ on the $\delta^{18}O_{fw}$ value that is used to calculate the relationship between $\delta^{18}O$ and salinity in the thermocline at this site. This reflects fact that *Risi et al*. [2010] show that their modeled $\delta^{18}O$ of precipitation is sensitive to the assumed sea surface temperature field. When using model-derived LGM sea surface temperatures they find no change in $\delta^{18}O$ of precipitation in this region versus a 4‰ change when CLIMAP sea surface temperatures are used as a model boundary condition. We use the published errors on the estimates of whole ocean $\delta^{18}O$ [*Schrag et al*., 2002] and salinity changes [*Insua et al*., 2014] that are used in calculating the LGM relationship between $\delta^{18}O$ and salinity in the thermocline. The measured values of $\delta^{18}O_{cib}$ at each core site in the vertical profile from off Australia are assigned an uncertainty of 0.07‰, which reflects the 1-sigma standard deviation of difference between the measured Holocene value and the value predicted from modern water column conditions for all core depths.

4. Results and Discussion

4.1. Vertical Profiles

A vertical profile of benthic foraminiferal $\delta^{18}O$ from south of Australia (Figure 3) shows that for both recent (Holocene) and LGM sediments, the oxygen isotope ratio increases with depth as seawater potential density increases, with little overall change in the vertical gradient. For both time periods, the denser waters south of the ACC are accompanied by higher $\delta^{18}O$ of benthic foraminifera, but the gradient in foraminiferal $\delta^{18}O$ across the ACC is slightly greater between 1 and 2.5 km during the LGM than for the recent sediments. If we assume that the gradients in $\delta^{18}O$ of benthic foraminifera represent the density gradients, we would infer

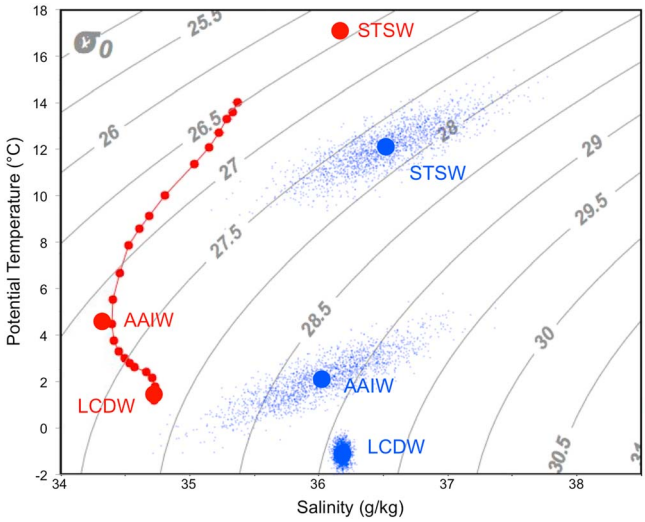

Figure 4. The *T* and *S* of the end-member values from each water mass used to interpolated the Australia margin $\delta^{18}O_{cib}$ values to density. Within the uncertainty ranges of the input parameters, the inferred salinity and density of AAIW are most sensitive to the value assumed for AAIW temperature. Thus, uncertainty in AAIW temperature is the largest source of uncertainty in the transport estimate.

little change or a slight increase in density stratification, which in models is tightly coupled to the strength of the ACC and AABW export (Figure 2).

However, we cannot simply interpret the change in $\delta^{18}O$ gradient as a change in density gradient, as it is probable that the relationship between foraminiferal $\delta^{18}O$ and density changed over time. In the upper ocean in tropical and temperate latitudes, the $\delta^{18}O$ in seawater can be related to salinity as both reflect freshwater cycling at the sea surface (evaporation and precipitation). At high latitudes the relationship between the $\delta^{18}O$ in seawater and salinity is complicated due to the additional effects of sea ice formation and melt which fractionate the isotopes very little, but can change the salinity greatly. For example, if enhance buoyancy extraction due sea ice formation and export led to higher salinity and denser Antarctic Bottom Waters, this would not necessarily be apparent in the $\delta^{18}O$ of the benthic foraminifera. Also complicating the use of the $\delta^{18}O$ in foraminiferal tests as a proxy for seawater density in the cold ocean is the fact that seawater density, but not the $\delta^{18}O$ in foraminifera, becomes less sensitive to temperature at colder temperatures. However, when we determine the contributions of temperature and seawater $\delta^{18}O$ to the foraminifera $\delta^{18}O$ signal and estimate how the relationship between salinity and seawater $\delta^{18}O$ changed with time using the methods described above, notion that the density gradients were not radically different during glacial times is supported.

4.2. LGM ACC Transport Estimate

Our best estimates for the LGM density structure across the ACC yield a transport increase of 18% with 1-sigma uncertainty on the LGM ACC transport estimate of 53% (116 ± 51 Sv for 0–3 km baroclinic transport, 186 ± 83 Sv for total transport; Table S5). The uncertainties in AAIW temperature and the $\delta^{18}O_{sw}$ and *S* assumed for the subtropical gyre account for much of the total error on the transport calculation (35 Sv of the 51 Sv). Considering the errors, this allows for a wide range in LGM ACC transport, from 30% reduction to almost double today's value.

Figure 4 shows how AAIW density estimates (and thus density along the entire Antarctic Margin) are impacted by uncertainties in AAIW temperature. More direct estimates of AAIW $\delta^{18}O_{sw}$ and *S* from pore waters could improve our estimates considerably. If we had a single pore water site at AAIW depths that could produce estimates of *T*, *S*, and $\delta^{18}O_{sw}$ of that are of the same accuracy as the Site 1123 LCDW site, the error on the transport estimate would be reduced to 14% (±17 Sv). Pore water-based estimates of *T* and $\delta^{18}O_{sw}$ do exist for 2500–2700 m water depth off Tasmania [*Malone et al.*, 2004], but salinity estimates are not available for these locations. However, it is worth noting that their reconstructed Holocene to LGM $\delta^{18}O_{sw}$ change (1.0 ± 0.15‰ at 2500 and 1.1 ± 0.15‰ at 2700 m, 95% confidence interval) overlaps with the value from our study for these water depths (1.01 ± 0.17‰). Unfortunately, these cores are too deep to provide a stronger constraint on AAIW properties than the ones used in this study.

4.3. Weakened Westerly Wind Scenario

While some mechanisms for CO_2 drawdown such as higher biological nutrient utilization in the subantarctic zone due to iron fertilization do not require circulation changes, other mechanisms call on a decrease in the physical exchange of deep and surface waters in the Antarctic, or the isolation of deep waters formed in the Antarctic from the atmosphere [*Hain et al.*, 2014; *Jaccard et al.*, 2013]. One scenario for explaining

the reduction in atmospheric CO_2 suggests that weakened westerly winds over the Antarctic during the LGM reduced Ekman upwelling and thus lead to increased efficiency in the drawdown of nutrients and carbon from the surface ocean by biological processes [*Toggweiler et al*., 2006]. Weaker wind forcing to the ACC can result from an overall weakening of the westerlies or a northward shift of the maximum westerlies (or both). Weaker Antarctic upwelling is consistent with the relatively weaker Antarctic productivity during the LGM [*Kohfeld et al*., 2005]. While the winds may provide much of the energy to drive the ACC, modern observations show that the tilt of the isopycnals is insensitive to the surface wind stress limited by the eddy activity [*Boning et al*., 2008]. Because the ACC is already thought to be in this "eddy saturated" state, a weakening in the winds over the Southern Ocean might not lead to a significant weakening of the ACC. So it is possible that a significant weakening of the winds over the Southern Ocean might not be reflected in the density contrast across the ACC. In an eddy resolving idealized model, *Morrison and Hogg* [2013] show that the meridional circulation (which is what matters for the atmospheric CO_2 drawdown mechanism) is more sensitive to wind changes than the zonal circulation. So our data leave open the possibility that wind-driven upwelling was significantly weaker during the LGM. However, because most of the energy supplied to the ACC by the winds is dissipated at the bottom of the ocean, the imprint of the weakened winds should be apparent as a decrease in near bottom kinetic energy. The grain size data of *McCave et al*. [2014] suggest no net change in the bottom current energy, and the magnetic grain size data in the Indian Ocean Sector also suggest an increase in bottom current energy [*Mazaud et al*., 2010]. However, recently published grain size measurements do suggest a reduction in bottom current energy in the northern edge of the Drake Passage [*Lamy et al*., 2015]. So while our density reconstruction cannot address whether wind-driven upwelling weakened, the sediment size data overall would suggest that changes in momentum input in to the ACC system would have been modest.

4.4. Isolated Antarctic Bottom Water Cell

Other scenarios for LGM Southern Ocean circulation call on enhanced sea ice cover in the Southern Ocean during the LGM. While today sea ice melts back seasonally to the Antarctic Continent, it expected that the cooler glacial climate caused an expansion of Southern Ocean Sea Ice. Microfossil-based reconstructions support an expansion of sea ice, as do most simulations using global climate models [*Gersonde et al*., 2005; *Otto-Bliesner et al*., 2006]. Permanent ice cover could help to lower atmospheric CO_2 by preventing the exchange of carbon between upwelled deep water and the atmosphere [*Stephens and Keeling*, 2000]. Observed depletion of radiocarbon in the deep water is consistent with a weak AABW ventilation and incomplete air-sea equilibration of CO_2 [*Skinner et al*., 2015]. Enhanced sea ice may have had profound effects on deep water circulation and properties as well. *Ferrari et al*. [2014] note that the position of the summer sea ice edge corresponds to the boundary between a region of surface buoyancy extraction (primarily through sea ice formation) to the south and surface buoyancy addition to the north. Thus, the ice edge determines the boundary between the circulation cell associated with AABW formation and the upper cell associated with NADW. The more northward position of the sea ice edge, coupled with the constraint on the eddy-saturated tilt of isopycnals across the ACC, would lead to a shoaling of the boundary between these cells during the LGM.

Enhanced buoyancy extraction south of the ice edge via sea ice formation and export, coupled with less ice shelf melting [*Miller et al*., 2012], also implies an increase in the density gradient across the ACC. As the newly formed AABW become saltier relative to the waters entering the Southern Ocean, this would create an increase in both the density gradient across the ACC and the vertical density gradient north of the ACC. Salinity of the LGM AABW increases relative to the modern condition across all of the PMIP2 models but its magnitude varies widely [*Weber et al*., 2007]. Some models predict a strong increase in the AABW salinity leading to the proportionally strong ACC transport and AABW formation.

In contrast, recent inverse modeling incorporating paleoceanographic tracer data implies a slow-down of AABW export during the LGM [*Gebbie*, 2014]. We also do not find support for the scenarios with an extreme change in density structure in our analysis. Scenarios with intense AABW formation would also seem to violate the observation that atmospheric CO_2 concentrations were lower during glacial times, as it would increase the preformed nutrient inventory and weaken the retention of biologically sequestered carbon in the deep ocean. Furthermore, a strong increase in density stratification and ACC transport is not supported by the grain size data [*McCave et al*., 2014], which would allow for only very modest increases in ACC strength. It is possible, however, that this mechanism might have been operating during the LGM, just not as strongly as exhibited in some of the models.

5. Conclusions

Models suggest a tight coupling between the lateral gradient in density across the ACC, the vertical gradient in density north of the ACC, ACC transport, and the strength and vertical extent of the AABW cell. In models that show an intensification of these gradients in transports during the LGM, the enhanced density gradient is driven by enhanced buoyancy extraction by sea ice formation in the Southern Ocean. Our best estimate of the vertical gradient in density north of the ACC suggests only a modest increase in ACC transport, but the uncertainty in this estimate is large.

Better constraints on the LGM Southern Ocean circulation, and the impact the circulation change may have had on atmospheric CO_2, will require better estimates of past LGM density. Additional information from pore waters at different water depths on both sides of the ACC would allow for a much more direct and robust flow estimate. But even a single pore water site that could provide information on past AAIW properties to same precision as existing deeper profiles could reduce the errors on our calculation significantly.

Acknowledgments
The authors acknowledge the US National Science Foundation (PLR-1345378). We also thank Andy Thompson, Jess Adkins, Ryan Abernathey, and the anonymous reviewers for their helpful discussions. All previously unpublished isotope data reported in this study are archived at World Data Center-A for Paleoclimatology located at the U.S. National Oceanic and Atmospheric Administration National Climatic Data Center Paleoclimatology Program, Boulder, Colorado (https://www.ncdc.noaa.gov/paleo/study/20022, https://www.ncdc.noaa.gov/paleo/study/19463) and in Tables S1–S4.

References

Adkins, J. F., and D. P. Schrag (2003), Reconstructing Last Glacial Maximum bottom water salinities from deep-sea sediment pore fluid profiles, *Earth Planet. Sci. Lett.*, *216*(1–2), 109–123.

Adkins, J. F., K. McIntyre, and D. P. Schrag (2002), The salinity, temperature, and $\delta^{18}O$ of the glacial deep ocean, *Science*, *298*(5599), 1769–1773.

Allison, L. C., H. L. Johnson, D. P. Marshall, and D. R. Munday (2010), Where do winds drive the Antarctic Circumpolar Current?, *Geophys. Res. Lett.*, *37*, L12605, doi:10.1029/2010GL043355.

Antonov, J. I., D. Seidov, T. P. Boyer, R. A. Locarnini, A. Mishonov, H. E. Garcia, O. K. Baranova, M. M. Zweng, and D. R. Johnson (2010), *World Ocean Atlas 2009, Volcume 2: Salinity*, 184 pp., AGU, Washington, D. C.

Boning, C. W., A. Dispert, M. Visbeck, S. R. Rintoul, and F. U. Schwarzkopf (2008), The response of the Antarctic Circumpolar Current to recent climate change, *Nat. Geosci.*, *1*(12), 864–869.

Bostock, H. C., et al. (2013), A review of the Australian-New Zealand sector of the Southern Ocean over the last 30 ka (Aus-INTIMATE project), *Quaternary Sci. Rev.*, *74*, 35–57.

Braconnot, P., et al. (2007), Results of PMIP2 coupled simulations of the Mid-Holocene and Last Glacial Maximum - Part 2: Feedback with emphasis on the location of the ITCZ and mid- and high latitudes heat budget, *Clim Past*, *3*(2), 279–296.

Calvo, E., C. Pelejero, P. De Deckker, and G. A. Logan (2007), Antarctic deglacial pattern in a 30 kyr record of sea surface temperature offshore south Australia, *Geophys. Res. Lett.*, *34*, L13707, doi:10.1029/2007GL029937.

Craig, H., and L. I. Gordon (1965), Deuterium and oxygen 18 variations in the ocean and the marine atmosphere: Stable isotopes in oceanographic studies and paleotemperatures, in *Proceedings of the Third Spoleto Conference, Spoleto, Italy*, edited by E. Tongiori, pp. 9–130, Sischi and Figli, Pisa.

Curry, W. B., and D. W. Oppo (2005), Glacial water mass geometry and the distribution of $\delta^{13}C$ of ΣCO_2 in the western Atlantic Ocean, *Paleoceanography*, *20*, PA1017, doi:10.1029/2004PA001021.

Duplessy, J. C., L. Labeyrie, and C. Waelbroeck (2002), Constraints on the ocean oxygen isotopic enrichment between the Last Glacial Maximum and the Holocene: Paleoceanographic implications, *Quaternary Sci. Rev.*, *21*(1–3), 315–330.

Elderfield, H., P. Ferretti, M. Greaves, S. Crowhurst, I. N. McCave, D. Hodell, and A. M. Piotrowski (2012), Evolution of ocean temperature and ice volume through the Mid-Pleistocene climate transition, *Science*, *337*(6095), 704–709.

Elmore, A. C., E. L. McClymont, H. Elderfield, S. Kender, M. R. Cook, M. J. Leng, M. Greaves, and S. Misra (2015), Antarctic Intermediate Water properties since 400 ka recorded in infaunal (*Uvigerina peregrina*) and epifaunal (*Planulina wuellerstorfi*) benthic foraminifera, *Earth Planet. Sci. Lett.*, *428*, 193–203.

Ferrari, R., M. F. Jansen, J. F. Adkins, A. Burke, A. L. Stewart, and A. F. Thompson (2014), Antarctic sea ice control on ocean circulation in present and glacial climates, *Proc. Natl. Acad. Sci. U.S.A.*, *111*(24), 8753–8758.

Ganachaud, A., and C. Wunsch (2000), Improved estimates of global ocean circulation, heat transport and mixing from hydrographic data, *Nature*, *408*, 453–457.

Gebbie, G. (2014), How much did Glacial North AtlanticWater shoal?, *Paleoceanography*, *29*, 190–209, doi:10.1002/2013PA002557.

Gersonde, R., X. Crosta, A. Abelmann, and L. Armand (2005), Sea-surface temperature and sea ice distribution of the Southern Ocean at the EPILOG Last Glacial Maximum—A circum-Antarctic view based on siliceous microfossil records, *Quaternary Sci. Rev.*, *24*(7–9), 869–896.

Gibbons, F. T., D. W. Oppo, M. Mohtadi, Y. Rosenthal, J. Cheng, Z. Y. Liu, and B. K. Linsley (2014), Deglacial $\delta^{18}O$ and hydrologic variability in the tropical Pacific and Indian Oceans, *Earth Planet. Sci. Lett.*, *387*, 240–251.

Goosse, H., and T. Fichefet (1999), Importance of ice-ocean interactions for the global ocean circulation: A model study, *J. Geophys. Res.*, *104*(C10), 23,337–23,355, doi:10.1029/1999JC900215.

Gordon, C., C. Cooper, C. A. Senior, H. Banks, J. M. Gregory, T. C. Johns, J. F. B. Mitchell, and R. A. Wood (2000), The simulation of SST, sea ice extents and ocean heat transports in a version of the Hadley Centre coupled model without flux adjustments, *Clim. Dyn.*, *16*(2–3), 147–168.

Grootes, P. M., E. J. Steig, M. Stuiver, E. D. Waddington, and D. L. Morse (2001), The Taylor dome Antarctic O-18 record and globally synchronous changes in climate, *Quatern. Res.*, *56*(3), 289–298.

Hain, M. P., D. M. Sigman, and G. H. Haug (2014), The biological pump in the past, in *Treatise on Geochemistry (Second Edition). Volume 8: The Oceans and Marine Geochemistry*, edited by M. J. Mottl and H. Elderfield, pp. 485–517, Elsevier, Amsterdam.

Hallberg, R., and A. Gnanadesikan (2006), The role of eddies in determining the structure and response of the wind-driven southern hemisphere overturning: Results from the Modeling Eddies in the Southern Ocean (MESO) project, *J. Phys. Oceanogr.*, *36*(12), 2232–2252.

Hasumi, H., and S. Emori (2004), *K-1 Coupled Model (MIROC) Description, K-1 Technical Report 1, Center for Climate System Research*, Univ. of Tokyo, Tokyo.

Hesse, T., M. Butzin, T. Bickert, and G. Lohmann (2011), A model-data comparison of $\delta^{13}C$ in the glacial Atlantic Ocean, *Paleoceanography*, *26*, PA3220, doi:10.1029/2010PA002085.

Hodell, D. A., C. D. Charles, J. H. Curtis, P. G. Mortyn, U. S. Ninnemann, and K. A. Venz (2003), Data report: Oxygen isotope stratigraphy of ODP Leg 177 Sites 1088, 1089, 1090, 1093, and 1094, in *Proc. ODP, Sci. Results*, edited by R. Gersonde et al., pp. 1–26, Ocean Drilling Program, College Station, Tex.

Holbourn, A., W. Kuhnt, and N. James (2002), Late Pleistocene bryozoan reef mounds of the Great Australian Bight: Isotope stratigraphy and benthic foraminiferal record, *Paleoceanography*, *17*(3), 1042, doi:10.1029/2001PA000643.

Howard, E., A. M. Hogg, S. Waterman, and D. P. Marshall (2015), The injection of zonal momentum by buoyancy forcing in a Southern Ocean model, *J. Phys. Oceanogr.*, *45*(1), 259–271.

Insua, T. L., A. J. Spivack, D. Graham, S. D'Hondt, and K. Moran (2014), Reconstruction of Pacific Ocean bottom water salinity during the Last Glacial Maximum, *Geophys. Res. Lett.*, *41*, 2914–2920, doi:10.1002/2014GL059575.

Jaccard, S. L., C. T. Hayes, A. Martinez-Garcia, D. A. Hodell, R. F. Anderson, D. M. Sigman, and G. H. Haug (2013), Two modes of change in Southern Ocean productivity over the past million years, *Science*, *339*(6126), 1419–1423.

Jacobs, S. S., P. A. Mele, W. M. Smethie, and R. A. Mortlock (2005), Summer oceanographic measurements near the Mertz Polynya (140–150°E) on N.B. Palmer cruise 00–08. Cruise report.

Johnson, G. C., and H. L. Bryden (1989), On the size of the Antarctic Circumpolar Current, *Deep Sea Res.*, *36*(1), 39–53.

Kohfeld, K. E., C. Le Quere, S. P. Harrison, and R. F. Anderson (2005), Role of marine biology in glacial-interglacial CO2 cycles, *Science*, *308*(5718), 74–78.

Labeyrie, L., et al. (1996), Hydrographic changes of the Southern Ocean (southeast Indian sector) over the last 230 kyr, *Paleoceanography*, *11*(1), 57–76, doi:10.1029/95PA02255.

Lamy, F., et al. (2015), Glacial reduction and millennial-scale variations in Drake Passage throughflow, *Proc. Natl. Acad. Sci. U.S.A.*, *112*(44), 13,496–13,501.

Locarnini, R. A., A. Mishonov, J. I. Antonov, T. P. Boyer, H. E. Garcia, M. M. Baranova, M. M. Zweng, and D. R. Johnson (2010), *World Ocean Atlas 2009, Volume 1: Temperature*, 184 pp., AGU, Washington, D. C.

Locarnini, R. A., et al. (2013), *World Ocean Atlas 2013, Volume 1: Temperature*, edited by S. Levitus, A. Mishonov Technical Ed., *NOAA Atlas NESDIS 73*, 40 pp.

Lynch-Stieglitz, J. (2015), *Southern Continental Margin of Australia Benthic Foraminifera Stable Isotope Data, Lynch-Stieglitz 2015*, National Centers for Environmental Information, NESDIS, NOAA, U.S. Department of Commerce, NOAA NCDC World Data Center for Paleoclimatology, Boulder, Colo. [Available at https://www.ncdc.noaa.gov/paleo/study/19463.]

Lynch-Stieglitz, J., and R. G. Fairbanks (1994), Glacial-interglacial history of Antarctic Intermediate Water - Relative strengths of Antarctic versus Indian-Ocean sources, *Paleoceanography*, *9*(1), 7–29, doi:10.1029/93PA02446.

Lynch-Stieglitz, J., W. B. Curry, and N. Slowey (1999), A geostrophic transport estimate for the Florida Current from the oxygen isotope composition of benthic foraminifera, *Paleoceanography*, *14*(3), 360–373, doi:10.1029/1999PA900001.

Lynch-Stieglitz, J., et al. (2007), Atlantic meridional overturning circulation during the Last Glacial Maximum, *Science*, *316*(5821), 66–69.

Mackensen, A. (1994), Benthic foraminiferal assemblages and the $\delta^{13}C$ signal in the Atlantic sector of the Southern Ocean: Glacial-to-interglacial contrasts, in *Carbon Cycling in the Glacial Ocean: Constraints on the Ocean's Role in Global Change*, edited by R. Zahn et al., pp. 105–144, North Atlantic Treaty Organization, Brussels, Belgium.

Mackensen, A., H. Grobe, H. W. Hubberten, V. Spiess, and D. K. Futterer (1989), Stable isotope stratigraphy from the Antarctic Continental Margin during the last one million years, *Mar. Geol.*, *87*(2–4), 315–321.

Mackensen, A., H. W. Hubberten, T. Bickert, G. Fischer, and D. K. Futterer (1993), The $\delta^{13}C$ in benthic foraminiferal tests of *Fontbotia-wuellerstorfi* (Schwager) relative to the $\delta^{13}C$ of dissolved inorganic carbon in Southern-Ocean deep-water - Implications for glacial ocean circulation models, *Paleoceanography*, *8*(5), 587–610, doi:10.1029/93PA01291.

Malone, M. J., J. B. Martin, J. Schönfeld, U. S. Ninnemann, D. Nürnburg, and T. S. White (2004), The oxygen isotopic composition and temperature of Southern Ocean bottom waters during the Last Glacial Maximum, *Earth Planet. Sci. Lett.*, *222*(1), 275–283.

Marchitto, T. M., and W. S. Broecker (2006), Deep water mass geometry in the glacial Atlantic Ocean: A review of constraints from trace metal paleonutrient proxies, *Geochem. Geophys. Geosyst.*, *7*, Q12003, doi:10.1029/2006GC001323.

Marchitto, T. M., W. B. Curry, J. Lynch-Stieglitz, S. P. Bryan, K. M. Cobb, and D. C. Lund (2014), Improved oxygen isotope temperature calibrations for cosmopolitan benthic foraminifera, *Geochim. Cosmochim. Acta*, *130*, 1–11.

Marti, O., et al. (2010), Key features of the IPSL ocean atmosphere model and its sensitivity to atmospheric resolution, *Clim. Dyn.*, *34*(1), 1–26.

Mashiotta, T. A., D. W. Lea, and H. J. Spero (1999), Glacial-interglacial changes in subantarctic sea surface temperature and $\delta^{18}O$ water using foraminiferal Mg, *Earth Planet. Sci. Lett.*, *170*(4), 417–432.

Masich, J., T. K. Chereskin, and M. R. Mazloff (2015), Topographic form stress in the Southern Ocean state estimate, *J. Geophys. Res. Oceans*, *120*, 7919–7933, doi:10.1002/2015JC011143.

Mazaud, A., E. Michel, F. Dewilde, and J. L. Turon (2010), Variations of the Antarctic Circumpolar Current intensity during the past 500 ka, *Geochem. Geophys. Geosyst.*, *11*, Q08007, doi:10.1029/2010GC003033.

Mazloff, M. R., R. Ferrari, and T. Schneider (2013), The force balance of the Southern Ocean Meridional Overturning Circulation, *J. Phys. Oceanogr.*, *43*(6), 1193–1208.

McCave, I. N., S. J. Crowhurst, G. Kuhn, C. D. Hillenbrand, and M. P. Meredith (2014), Minimal change in Antarctic Circumpolar Current flow speed between the last glacial and Holocene, *Nat. Geosci.*, *7*(2), 113–116.

McCorkle, D. C., D. T. Heggie, and H. H. Veeh (1998), Glacial and Holocene stable isotope distributions in the southeastern Indian Ocean, *Paleoceanography*, *13*(1), 20–34, doi:10.1029/97PA02305.

Meredith, M. P., and A. M. Hogg (2006), Circumpolar response of Southern Ocean eddy activity to a change in the Southern Annular Mode, *Geophys. Res. Lett.*, *33*, L16608, doi:10.1029/2006GL026499.

Miller, M. D., J. F. Adkins, D. Menemenlis, and M. P. Schodlok (2012), The role of ocean cooling in setting glacial southern source bottom water salinity, *Paleoceanography*, *27*, PA3207, doi:10.1029/2012PA002297.

Morrison, A. K., and A. M. Hogg (2013), On the relationship between Southern Ocean overturning and ACC transport, *J. Phys. Oceanogr.*, *43*(1), 140–148.

Moy, A. D., W. R. Howard, and M. K. Gagan (2006), Late Quaternary palaeoceanography of the circumpolar deep water from the South Tasman Rise, *J. Quaternary Sci.*, *21*(7), 763–777.

Munday, D. R., L. C. Allison, H. L. Johnson, and D. P. Marshall (2011), Remote forcing of the Antarctic Circumpolar Current by diapycnal mixing, *Geophys. Res. Lett.*, *38*, L08609, doi:10.1029/2011GL046849.

Munday, D. R., H. L. Johnson, and D. P. Marshall (2013), Eddy saturation of equilibrated circumpolar currents, *J. Phys. Oceanogr.*, *43*(3), 507–532.
Ninnemann, U. S., and C. D. Charles (2002), Changes in the mode of Southern Ocean circulation over the last glacial cycle revealed by foraminiferal stable isotopic variability, *Earth Planet. Sci. Lett.*, *201*(2), 383–396.
Opsteegh, J. D., R. J. Haarsma, F. M. Selten, and A. Kattenberg (1998), ECBILT: A dynamic alternative to mixed boundary conditions in ocean models, *Tellus A*, *50*(3), 348–367.
Orsi, A. H., T. Whitworth, and W. D. Nowlin (1995), On the meridional extent and fronts of the Antarctic Circumpolar Current, *Deep-Sea Res. Pt I*, *42*(5), 641–673.
Ostermann, D. R., and W. B. Curry (2000), Calibration of stable isotopic data: An enriched $\delta^{18}O$ standard used for source gas mixing detection and correction, *Paleoceanography*, *15*(3), 353–360, doi:10.1029/1999PA000411.
Ostlund, H. G., H. Craig, W. S. Broecker, and D. Spenser (1987), *GEOSECS Atlantic, Pacific and Indian Ocean Expeditions Vol. 7, Shorebased Data and Graphics*, 200 pp., National Science Foundation, Washington, D. C.
Ott, G., and R. Gersonde (1997a), Sedimentology and stable isotopes on core PS1649-2, doi:10.1594/PANGAEA.51770.
Ott, G., and R. Gersonde (1997b), Sedimentology and stable isotopes on core PS1436-1, doi:10.1594/PANGAEA.51768.
Otto-Bliesner, B. L., E. C. Brady, G. Clauzet, R. Tomas, S. Levis, and Z. Kothavala (2006), Last Glacial Maximum and Holocene climate in CCSM3, *J. Climate*, *19*, 2526–2544.
Passlow, V., P. X. Wang, and A. R. Chivas (1997), Late Quaternary palaeoceanography near Tasmania, southern Australia, *Palaeogeography Palaeoclimatology Palaeoecology*, *131*(3–4), 433–463.
Rintoul, S. R., and S. Sokolov (2001), Baroclinic transport variability of the Antarctic Circumpolar Current south of Australia (WOCE repeat section SR3), *J. Geophys. Res.*, *106*(C2), 2815, doi:10.1029/2000JC900107.
Risi, C., S. Bony, F. Vimeux, and J. Jouzel (2010), Water-stable isotopes in the LMDZ4 general circulation model: Model evaluation for present-day and past climates and applications to climatic interpretations of tropical isotopic records, *J. Geophys. Res-Atmos.*, *115*, D24123, doi:10.1029/2009JD013255.
Roberts, J., J. Gottschalk, L. C. Skinner, V. L. Peck, S. Kender, H. Elderfield, C. Waelbroeck, N. V. Riveiros, and D. A. Hodell (2016), Evolution of South Atlantic density and chemical stratification across the last deglaciation, *Proc. Natl. Acad. Sci. U.S.A.*, *113*(3), 514–519.
Ronge, T. A., S. Steph, R. Tiedemann, M. Prange, U. Merkel, D. Nürnberg, and G. Kuhn (2015), Pushing the boundaries: Glacial/interglacial variability of intermediate and deep waters in the southwest Pacific over the last 350,000 years, *Paleoceanography*, *30*, 23–38, doi:10.1002/2014PA002727.
Schmidt, G. A., G. R. Bigg, and E. J. Rohling (1999), Global Seawater Oxygen-18 Database - v1.21, National Aeronautics and Space Administration, Goddard Institute for Space Studies. [Available at http://data.giss.nasa.gov/o18data/.]
Schrag, D. P., J. F. Adkins, K. McIntyre, J. L. Alexander, D. A. Hodell, C. D. Charles, and J. F. McManus (2002), The oxygen isotopic composition of seawater during the Last Glacial Maximum, *Quaternary Sci. Rev.*, *21*(1–3), 331–342.
Sikes, E. L., W. R. Howard, C. R. Samson, T. S. Mahan, L. G. Robertson, and J. K. Volkman (2009), Southern Ocean seasonal temperature and subtropical front movement on the South Tasman Rise in the late Quaternary, *Paleoceanography*, *24*, PA2201, doi:10.1029/2008PA001659.
Skinner, L., I. N. McCave, L. Carter, S. Fallon, A. E. Scrivner, and F. Primeau (2015), Reduced ventilation and enhanced magnitude of the deep Pacific carbon pool during the last glacial period, *Earth Planet. Sci. Lett.*, *411*, 45–52.
Stephens, B. B., and R. F. Keeling (2000), The influence of Antarctic sea ice on glacial-interglacial CO2 variations, *Nature*, *404*(6774), 171–174.
Toggweiler, J. R., J. L. Russell, and S. R. Carson (2006), Midlatitude westerlies, atmospheric CO2, and climate change during the ice ages, *Paleoceanography*, *21*, PA2005, doi:10.1029/2005PA001154.
Waelbroeck, C., et al. (2009), Constraints on the magnitude and patterns of ocean cooling at the Last Glacial Maximum, *Nat. Geosci.*, *2*(2), 127–132.
Weber, S. L., S. S. Drijfhout, A. Abe-Ouchi, M. Crucifix, M. Eby, A. Ganopolski, S. Murakami, B. Otto-Bliesner, and W. R. Peltier (2007), The modern and glacial overturning circulation in the Atlantic Ocean in PMIP coupled model simulations, *Clim. Past*, *3*(1), 51–64.
Zweng, M. M., et al. (2013), *World Ocean Atlas 2013, Volume 2: Salinity*, edited by S. Levitus, 39 pp., A. Mishonov Technical Ed., Silver Spring, *NOAA Atlas NESDIS 73*, 40 pp.